RESEARCH PAPER

Iopamidol-loaded dendrimers for enhanced computed tomography imaging: synthesis, characterization, and in vivo evaluation

Parsa Chehregani Rad [1], Tahereh Zadeh Mehrizi [2*], Mehdi Shafiee Ardestani [1,3*], Mehdi Mirzaei [4], Morteza Pirali Hamedani [5], Ahmad Javanmard [6], Mouzhan Rasoulianshiadehi [1]

[1] Department of Radiopharmacy, Faculty of Pharmacy, Tehran University of Medical Sciences, Tehran, Iran
[2] Health Management and Economics Research Center, Health Management Research Institute, Iran University of Medical Sciences, Tehran, Iran
[3] Research Center for Nuclear Medicine, Shariati Hospital, Tehran, Iran
[4] Iran Ministry of Health and Medical Education, Deputy Ministry for Education, Tehran, Iran
[5] Department of Medicinal Chemistry, Faculty of Pharmacy, Tehran University of Medical Sciences, Tehran, Iran
[6] Cancer Research Center, Shahid Beheshti University of Medical Sciences, Tehran, Iran

ABSTRACT

Objective(s): This study evaluated second-generation anionic linear globular dendrimers (G2-ALGD) as a nanocarrier platform to improve the physicochemical properties, imaging performance, and safety profile of iopamidol.

Materials and Methods: G2-ALGDs were synthesized via polyethylene glycol (PEG)-citric acid coupling and passively loaded with iopamidol (D-IPM). The formulation was characterized by Dynamic Light Scattering (DLS), Fourier transform infrared spectroscopy (FT-IR), and Transmission electron microscopy (TEM). In vitro drug release was assessed at pH 5.8 and 7.4. Long-term stability was evaluated over 90 days under different storage conditions. Cytocompatibility was assessed using an MTT assay in HEK-293 cells, and imaging performance was evaluated by micro-computed tomography (micro-CT) in Balb/c mice.

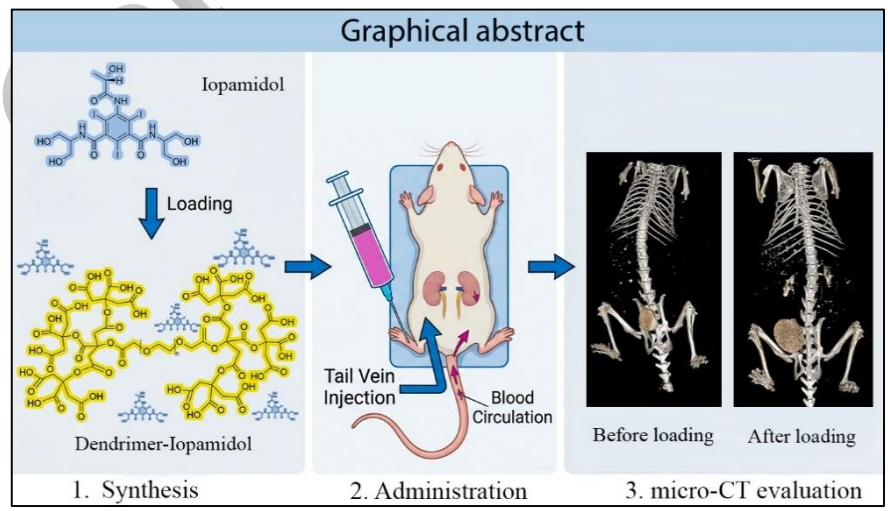
Results: Iopamidol loading increased particle size from 102.9 ± 8.7 to 129.8 ± 10.4 nm and shifted the zeta potential from −27.33 ± 1.75 to −0.07 ± 1.28 mV. FT-IR confirmed successful loading, while TEM revealed enhanced crystallinity. Drug encapsulation efficiency reached 43%. Drug release was pH-dependent, with significantly greater release at pH 5.8 ($p < 0.0001$). The formulation remained stable under refrigerated and lyophilized conditions but degraded at room temperature after 30 days. D-IPM was non-cytotoxic at concentrations ≤125 µg/mL. D-IPM also produced greater CT contrast (3985.06 ± 312.9 vs. 2483.61 ± 215.4 HU) and prolonged in vivo retention, evidenced by reduced bladder accumulation.

Conclusions: Dendrimer-loaded iopamidol demonstrated improved biocompatibility, stability, and CT imaging performance, highlighting its potential as a next-generation CT contrast agent.

Keywords: *Dendrimers; Iopamidol; Tomography; Cytocompatibility; Contrast media*

How to cite this article

Chehregani Rad P, Zadeh Mehrizi T, Shafiee Ardestani M, Mirzaei M, Pirali Hamedani M, Javanmard A, Rasoulianshiadehi M. Iopamidol-loaded dendrimers for enhanced computed tomography imaging: synthesis, characterization, and in vivo evaluation. Nanomed J. 2027; 14: 1-. doi: 10.22038/nmj.2026.97053.2450



* *Corresponding author(s):* **Tahereh Zadeh Mehrizi**, PhD, Health Management and Economics Research Center, Health Management Research Institute, Iran University of Medical Sciences, Tehran, Iran. Phone: +98 2188782919, Email: *taherehzadehmehrizi@gmail.com*; *Mehrizi.t@iums.ac.ir*; **Mehdi Shafiee Ardestani**, PhD, Department of Radiopharmacy, Faculty of Pharmacy, Tehran University of Medical Sciences, Tehran, Iran. Phone: +98 2164122103, Email: *shafieeardestani@gmail.com*.

Note. This manuscript was submitted on July 02, 2026; approved on August 29, 2026.

© 2026. This work is openly licensed via CC BY 4.0. This is an Open Access article distributed under the terms of the Creative Commons Attribution License (https://creativecommons.org/licenses), which permits unrestricted use, distribution, and reproduction in any medium, provided the original work is properly cited.

INTRODUCTION

Computed tomography (CT) scanning is a critical diagnostic imaging modality for real-time visualization of vascular anatomy (1, 2). Intravenous administration of iodinated contrast media (ICM) enhances image contrast, improving the differentiation of adjacent anatomical structures (3, 4). These contrast agents are classified based on their ionic nature (ionic vs. non-ionic), molecular size (monomeric or dimeric), osmolality, iodine content, and viscosity (4-6). These physicochemical characteristics strongly influence both imaging performance and safety (4, 6, 7).

High-osmolality contrast agents (HOCM), with an osmolality greater than 1500 mOsm/kg, have largely been replaced by low-osmolality contrast media (LOCM) and iso-osmolar contrast media (IOCM) because they have been associated with higher rates of adverse effects, including nephrotoxicity (8-11). LOCMs, such as iopamidol, with osmolarities of 300–900 mOsm/kg, have been found to be associated with a lower risk of contrast-induced nephropathy (CIN) compared with HOCMs (8, 12). Iopamidol also provided superior cost and safety profiles for high-risk nephropathy patients compared to other low-osmolality contrast agents. Despite these advantages, their short intravascular half-life requires relatively high or repeated doses to achieve sufficient image contrast. This increases the patient's exposure to iodine. This, in turn, increases the risk of side effects such as nephrotoxicity (13-16). Therefore, efforts have been made to develop new contrast agents with reduced viscosity and osmolality and increased half-life to limit these risks.

Nanoparticle-based contrast agents are among multiple new alternatives to conventional ICAs with enhanced safety profiles and advanced imaging capabilities. Among a wide range of nanoparticle platforms, dendrimer-based nanoparticles have been of particular interest due to their structural and functional properties, including prolonged systemic circulation, target delivery, and reduced toxicity (17-19). Dendrimers are nanoscale, monodisperse polymers with a highly branched structure, well-defined internal cavities for drug encapsulation, and a functional group-rich surface for conjugation of imaging agents (20-25). This structural versatility makes dendrimers ideal candidates for theranostic applications, wherein diagnostic imaging and targeted therapy can be coupled on a single nanoplatform (26, 27). In particular, second-generation anionic linear globular dendrimers (G2-ALGD), which were synthesized via biocompatible and biodegradable building blocks such as citric acid and polyethylene glycol (PEG), have shown high potential for biomedical applications (26, 28-30). The dendrimers reveal good physicochemical characteristics such as water solubility, negative surface charge, and significant drug-loading ability, which all contribute toward increased solubilization of hydrophobic drugs, release profiles, and minimized cytotoxicity (23, 31-35). These features reflect the promise of G2-ALGD as a multi-functional platform for the synthesis of the next-generation contrast agents.

In this work, we investigated the synergistic effects of G2-ALGD on the physicochemical and imaging properties of iopamidol. By loading iopamidol with G2-ALGD, we aimed to enhance its contrast efficacy while reducing potential nephrotoxicity, thereby supporting the development of safer and better CT imaging probes.

MATERIALS AND METHODS

Materials

Dicarboxylated polyethylene glycol (PEG-600; Merck, Germany), dimethylformamide (DMF; Chemex, China), N,N′-dicyclohexylcarbodiimide (DCC; Sigma-Aldrich, USA), citric acid (Merck, Germany), Sephadex G-50 (GE Healthcare Life Sciences, UK), high-glucose Dulbecco's Modified Eagle Medium (DMEM; Merck, Germany), fetal bovine serum (FBS; Merck, Germany), and dimethyl sulfoxide (DMSO; Sigma-Aldrich, USA) were used in this study. Human Embryonic Kidney 293 (HEK-293) cell line and six-month-old male Balb/c mice were purchased from the Pasteur Institute of Iran for *in vivo* and *in vitro* studies, respectively. Chemicals and reagents were of analytical grade and used without purification.

Synthesis of G2-ALGDs

Synthesis of dendrimers was performed as explained previously (36). In short, 0.2 g of calcium chloride and 2 mL of PEG-600 were mixed with 5 mL of anhydrous DMF. The mixture was stirred at room temperature for 15 min, then 0.15 g each of DCC and citric acid were added. An additional 0.15 g of DCC and 0.15 g of citric acid were added after 1 h, and the reaction mixture was stirred for 10 days at room temperature in a sealed flask. The synthesized G2-ALGDs were filtered through filter paper and purified on a Sephadex G-50 column to eliminate unreacted citric acid and DCC.

Iopamidol Loading onto the Dendrimers

The prepared dendrimers were dissolved in deionized water to a total volume of 6 mL. For drug loading, fixed amounts of dendrimer were mixed with different concentrations of Iopamidol to

Corrected Proof

determine the optimal loading conditions. The highest encapsulation efficiency was achieved by mixing 2 mL of the dendrimer solution with Iopamidol (300 mg I/mL) in a 50 mL vial. The mixture was incubated under gentle stirring for 2 h to facilitate the adsorption of Iopamidol molecules onto the dendrimer branches.

Determination of Drug encapsulation Efficiency

To determine the encapsulation efficiency of iopamidol onto the dendrimer, a calibration curve was initially prepared by measuring the absorbance of varying concentrations of iopamidol at 265 nm using an ultraviolet-visible (UV-Vis) spectrophotometer (Shimadzu, Japan). To separate free iopamidol from the dendrimer–drug complex, the 2 mL mixture was centrifuged at 10,000 rpm for 15 min. Supernatant absorbance was measured at 265 nm, and free iopamidol concentration was determined using the calibration curve equation. Drug concentration bound to the dendrimer (BD) was obtained using the following equation:

BD = TDA - FDS

Where TDA is the initial concentration of iopamidol, FDS is the free (unbound) drug in the supernatant, and BD is the drug bound to the dendrimer. Finally, the drug encapsulation efficiency (EE%) was calculated by the equation:

EE% = [(Total drug added – Free unentrapped drug) / Total drug added] × 100

Physicochemical Characterization of the Dendrimer and Dendrimer–Drug Complex

To confirm that the dendrimer synthesis was complete, drug loading was measured, and the physicochemical characteristics (e.g., size, charge, and molecular integrity) were evaluated using DLS, zeta sizer, FT-IR, and TEM.

For DLS and zeta potential measurements, 1.2 mL of the synthesized dendrimers and 1.2 mL of the dendrimer–drug complexes were prepared separately. For zeta potential measurement, 0.1 mL of each was used. Samples were transferred into disposable measurement cells, and the experiments were performed under a Horiba Scientific SZ-100 nanoparticle analyzer (Japan) at room temperature.

In addition, FT-IR spectroscopy was also performed in the liquid phase at room temperature. Briefly, 1.5 mL of each sample was placed in an AgCl cell and scanned by a Thermo Nicolet Avatar FT-IR spectrometer (USA). The infrared transmission spectra were scanned in the range 400–4000 cm^{-1} for both dendrimers and dendrimer–drug complexes.

Morphological characterization was finally carried out using a transmission electron microscope (CM120, Philips, Netherlands). Sample preparation involved copper grids coated with a carbon film. In brief, 5–10 µL of each sample was loaded on the grid and allowed to settle for 1–2 min. Excess liquid was carefully removed with filter paper before imaging.

In Vitro Drug Release Study

In order to find the release profile of iopamidol from the dendrimer, the dendrimer-drug complex was first centrifuged at 10,000 rpm for 15 min to pellet the drug bound to the dendrimer. The pellet was then resuspended in 1 mL of phosphate-buffered saline (PBS) and transferred to a dialysis bag with a molecular weight of 500–1000 daltons (Spectrum Laboratories, USA). Free drug molecules were permitted to dialyze freely through the membrane, but the dendrimer-drug complex was restrained. The bag was placed in a cylinder containing 100 mL of PBS and was kept stirred continuously with the help of a magnetic stirrer. Subsequently, at predetermined intervals of time (0, 2, 4, 6, 8, 10, 12, 24, and 48 h), 2 mL of the sample was removed from the release medium and replenished instantaneously with an identical volume of fresh PBS. The release rate of each sample was analyzed using a non-polar UV-Vis spectrophotometer at 265 nm against a standard calibration curve. The overall release of iopamidol was determined and graphed against time. Release of the drug was ascertained at pH 5.8 and 7.4 to mimic the cancer cell acidic microenvironment and physiological pH, respectively.

Stability Assessment of the Dendrimer–Drug Complex

The stability of the dendrimer-drug complex was evaluated by measuring changes in hydrodynamic size using the DLS method. Stability was established under various storage conditions, i.e., lyophilized form, refrigeration (2–8 °C), and room temperature (25 °C). The samples were analyzed at definite time points: 0 (after immediate synthesis), 3, 7, 30, and 90 days post-storage. At each time point and condition, 1.2 mL of dendrimer–drug complex was transferred to disposable cuvettes compatible with DLS measurement. The samples were analyzed on a Horiba Scientific SZ-100 nanoparticle analyzer (Japan) at room temperature.

Cytotoxicity Testing

The cytotoxicity of dendrimer–drug complexes and free iopamidol against HEK-293 cells was assessed by the MTT assay for a concentration range of 7.8, 15.6, 31.3, 62.5, 125, 250, and 500 µg/mL. Briefly, HEK-293 cells were plated in 96-well plates at a cell density of 5–10 × 10^3 cells/well in 100 µL of complete culture medium, and incubated for 24 h for

Corrected Proof

cell adhesion. After incubation, the medium was discarded, and 100 µL of the target test concentration was added to each well. The plates were incubated for 48 h. Afterwards, 20 µL of the MTT solution (5 mg/mL PBS) was added to each well and incubated at room temperature for 3–4 h to allow formazan crystallization. After incubation, the supernatant was removed, and 100 µL of DMSO was added per well and agitated vigorously for 5–10 min to dissolve the precipitated formazan crystals. Absorbance was measured at 570 nm using a microplate reader (Agilent BioTek, USA). Cell viability was approximated by using the following formula:

$$Viability\ (\%) = \frac{\text{Absorbance of treated cells}}{\text{Absorbance of control cells}} \times 100$$

Contrast Enhancement Assessment: Dendrimer–Iopamidol Complex vs. Free Iopamidol

In Vitro Study

In vitro phantom experiments were performed to compare the X-ray attenuation properties of the synthesized dendrimer–iopamidol complex with free iopamidol. Briefly, 0.5 mL of free iopamidol solution (306 mg of iopamidol and 150 mg of iodine) and an equivalent volume of dendrimer–iopamidol complex were each diluted at a ratio of 1:1 with deionized water. Deionized water alone was employed as a negative control. All samples were loaded into separate micro-CT sample holders and scanned under identical imaging conditions. The imaging parameters were set as follows: tube voltage of 50 kV, tube current of 150 µA, frame exposure time of 0.5 s, and 2× optical magnification. Acquisition duration was 30 min, with a reconstructed slice thickness of 25 µm. Image acquisition was performed using LOTUS-inVivo-ACQ software. Images were reconstructed using the Feldkamp-Davis-Kress (FDK) algorithm in LOTUS-inVivo-REC software and RadiAnt DICOM Viewer 25.1. Hounsfield Unit (HU) measurements were performed on reconstructed CT images using RadiAnt DICOM Viewer (version 25.1). For each phantom sample and organ, a region of interest (ROI) was manually drawn within a homogeneous area while avoiding boundaries and imaging artifacts. The mean HU value within each ROI was recorded. Measurements were performed in triplicate using identical ROI selection criteria, and the average value was used for statistical analysis. The HU values of the dendrimer–iopamidol complex and free iopamidol were then compared to ascertain their relative radiodensity enhancement.

In Vivo Study

All animal experiments adhered to the institutional ethical guidelines and were approved by Tehran University of Medical Sciences' Ethics Committees (Approval Code: IR.TUMS.AEC.1403.204) and Iran University of Medical Sciences' Ethics Committees (Approval Code: IR.IUMS.REC.1403.561). Imaging experiments were performed using the LOTUS-inVivo micro-CT system. Relative *in vivo* efficacy of dendrimer–iopamidol complex compared with free iopamidol was assessed in 6-month-old male Balb/c mice (n = three per group). Animals were anesthetized by inhalation with isoflurane and injected intravenously with either 0.2 mL of free iopamidol or dendrimer–iopamidol complex via the tail vein. The delivered dose was 122.4 mg of iopamidol and 60 mg of iodine. Baseline (0 min) and delayed images at 90 min were acquired to assess the distribution and retention of the contrast agent in all organs. The imaging parameters were identical to those employed in *in vitro* phantom scanning. Quantitative assessment of enhancement was made post-acquisition using measurement of the mean Hounsfield Unit (HU) within predefined regions of interest (ROIs) of the vital tissues. All measurements were performed in triplicate for consistency. HU values obtained from the free iopamidol and dendrimer–iopamidol groups were compared to determine differences in contrast enhancement and retention profiles over time.

Statistical Analysis

All graph presentations were plotted using GraphPad Prism version 10.0 (GraphPad Software, San Diego, CA, USA). Statistical analyses were performed using SigmaPlot version 15.0 (Systat Software, San Jose, CA, USA). Data are expressed as mean ± standard deviation (SD) from at least three independent experiments. For the comparison of more than two groups, one-way analysis of variance (ANOVA) followed by Tukey's post hoc test was applied. Pairwise comparisons were performed using Student's t-test where appropriate. A p-value of ≤ 0.05 was considered statistically significant.

RESULTS

Particle Size and Surface Charge Characterization

Fig. 1a shows the particle size distribution, whereas Fig. 1b presents the zeta potential values of dendrimers (D) and dendrimer–iopamidol complexes (D-IPM). After iopamidol loading, the particle size increased from 102.9 ± 8.7 nm for dendrimers to 129.8 ± 10.4 nm for D-IPM nanoparticles, indicating successful drug encapsulation.

Corrected Proof

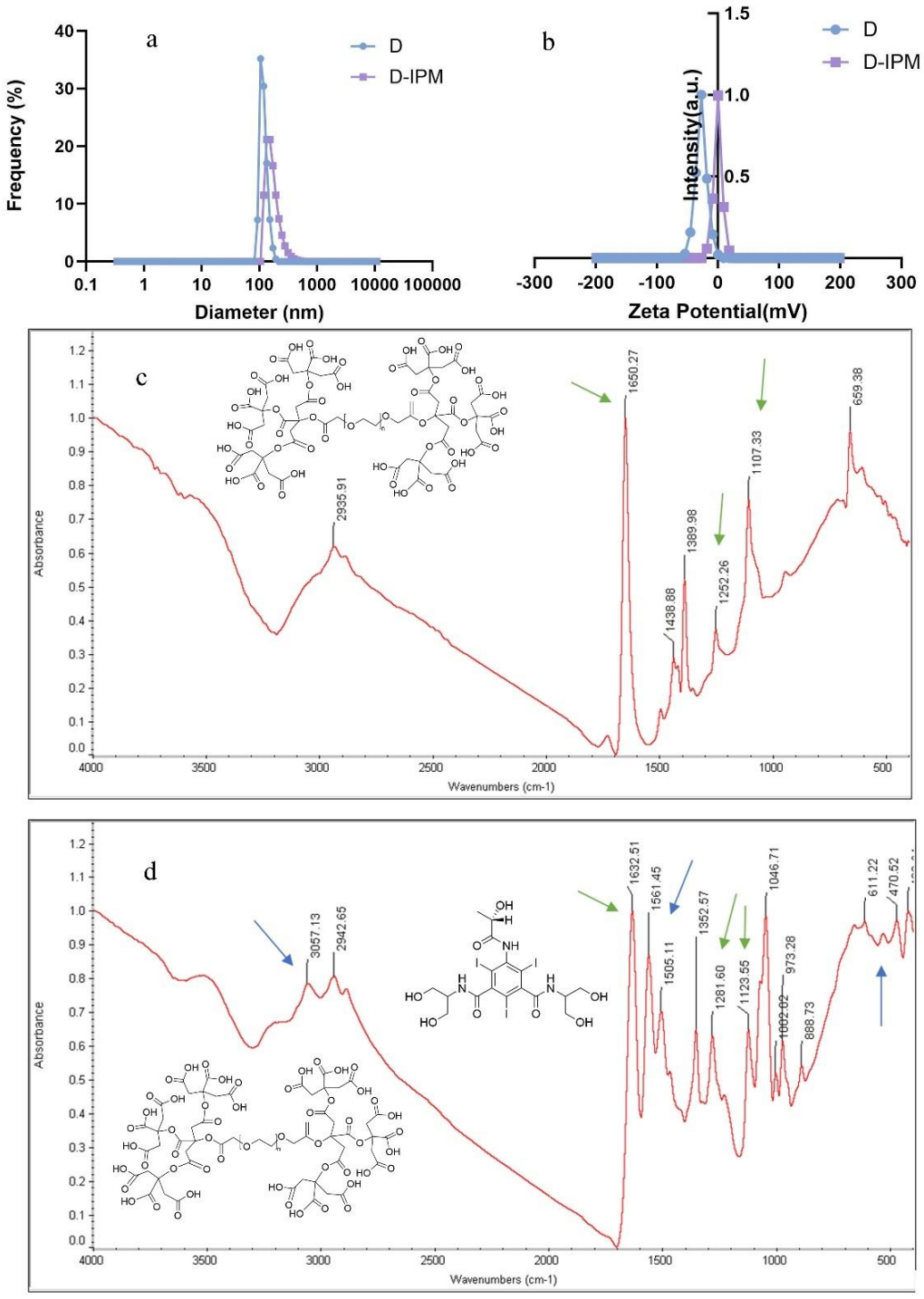


Fig. 1. (a) Hydrodynamic diameter and (b) zeta potential values of the dendrimer (D) and dendrimer–iopamidol complex (D-IPM). FTIR spectrum of (c) D and (d) D-IPM (green arrows indicate characteristic peaks corresponding to the dendrimer structure, while blue arrows highlight peaks specific to iopamidol functional groups).

In addition, zeta potential was altered from -27.33 ± 1.75 mV to -0.07 ± 1.28 mV, suggesting a loss of surface charge. The nearly neutral zeta potential of D-IPM suggests effective surface coverage, likely resulting from the neutral nature of iopamidol and the shielding effect of PEG. This finding is contrary to another PEG-based ICM, namely poly(methacrylated iopamidol)-polyethylene glycol-cRGD system (PMAI-PEG-RGD), which displayed more negative zeta potentials (−9.6 to −13.6 mV) due to charged peptide conjugation and polymer structure (37). The neutral surface charge of D-IPM is advantageous in reducing opsonization and prolonging circulation time (38).

Table 1. Size Distribution data of both dendrimers and dendrimer-iopamidol complexes.

Nanoparticle	Zeta potential (mV)	Size (nm)	PDI
Dendrimer (D)	-27.33 ± 1.75	102.9 ± 8.7	0.05
Dendrimer–Iopamidol (D-IPM)	-0.07 ± 1.28	129.8 ± 10.4	0.21

The polydispersity index (PDI) remained within the acceptable range, increasing from 0.05 for dendrimers to 0.21 for D-IPM after drug loading. Data are given in Table 1. Similarly, Fu et al. (39) reported the synthesis of high-yield, exceptionally monodisperse PEG-core dendritic conjugates of iobitridol. These conjugates exhibited favorable CT imaging profiles that included prolonged blood half-life (~35 min) and high aqueous solubility (>550 mg/mL at 25 °C). The dendrimers described by Fu et al. possessed a hydrodynamic profile akin to high-molecular-weight proteins and maintained excellent monodispersity (PDI < 1.04) (39). Interestingly, both systems showed an increase in hydrodynamic diameter after drug loading, supporting efficient drug encapsulation. The findings of Fu et al. highlighted the importance of PEG chain length on the particle size of the nanocomplexes (PEG3400 < PEG6000 < PEG12000) (39). Moreover, the size of dendrimer-iopamidol complex was smaller than PEGylated poly(iohexol) NPs (150 nm), albumin-based iohexol nanoparticles (254 nm), and iodinated polymer nanoparticles (147 nm) (40-42); however, it was larger than iodine-doped carbon dots (4 nm) (43).

FTIR Spectral Analysis

FTIR spectroscopy was performed to identify functional groups and confirm the successful loading of iopamidol onto the dendrimer. The spectra revealed characteristic peaks associated with interactions between the dendrimer and iopamidol (Fig. 1c and 2d). A peak at 3057.13 cm^{-1}, observed in the spectrum of the dendrimer–iopamidol complex alone, was attributed to N–H stretching vibrations of the amide groups of iopamidol, indicating successful loading. Broad O–H stretching vibration bands at 2935.91 cm^{-1} and 2942.65 cm^{-1} were assigned to hydroxyl groups of the dendrimer backbone and iopamidol.

The carbonyl (C=O) stretching vibration of the terminal citric acid groups in the free G2-ALGD dendrimer appeared as a sharp band at 1650.27 cm^{-1}. Upon loading with iopamidol, the band shifted to 1632.51 cm^{-1}, indicating hydrogen bonding and other interactions between iopamidol and dendrimer molecules. Two additional peaks at 1505.11 and 1561.45 cm^{-1} were observed only in the dendrimer–iopamidol complex. These peaks were assigned to aromatic C=C vibrations and the amide II bands of iopamidol, further confirming successful loading.

Bands at 1252.26 and 1281.60 cm^{-1} were attributed to ester bond vibrations associated with the citric acid linkages in the first- and second-generation ALGD structure. Ether bond vibrations of the dendrimer backbone were observed at 1107.33 cm^{-1} and 1123.55 cm^{-1}. Peaks at 479.52 cm^{-1} and 611.22 cm^{-1} were due to C–I stretching vibrations and identified as iodine-containing bonds.

Collectively, these findings confirm the successful functionalization of the dendrimer with iopamidol. Similarly, in the study on PMAI-PEG-RGD (37), successful stepwise synthesis and surface modification were also verified by characteristic carbonyl (1642 cm^{-1}) and amide (1547 cm^{-1}) stretching peaks. Although both systems exhibited retention of principal functional groups following synthesis, our FTIR spectra revealed aromatic C=C and ester/ether bond vibrations, indicating a more complex dendrimer–drug interaction.

TEM Imaging Data

Representative TEM images are given in Fig. 2a and 2b. After iopamidol loading, the dendrimers exhibited a more ordered and crystalline morphology, suggesting successful drug loading and surface organization. Particle size analysis using TEM images showed an increased average diameter upon the addition of iopamidol. Specifically, the native dendrimer had an average particle size of 9.2 nm, while that of the dendrimer–iopamidol complex was 10.8 nm, corresponding to an increase of 1.6 nm. A full-size distribution of the nanoparticles is presented in the histogram (Fig. 2c) and the violin plot (Fig. 2d), illustrating the homogeneity and range of particle sizes both before and after iopamidol loading.

Corrected Proof

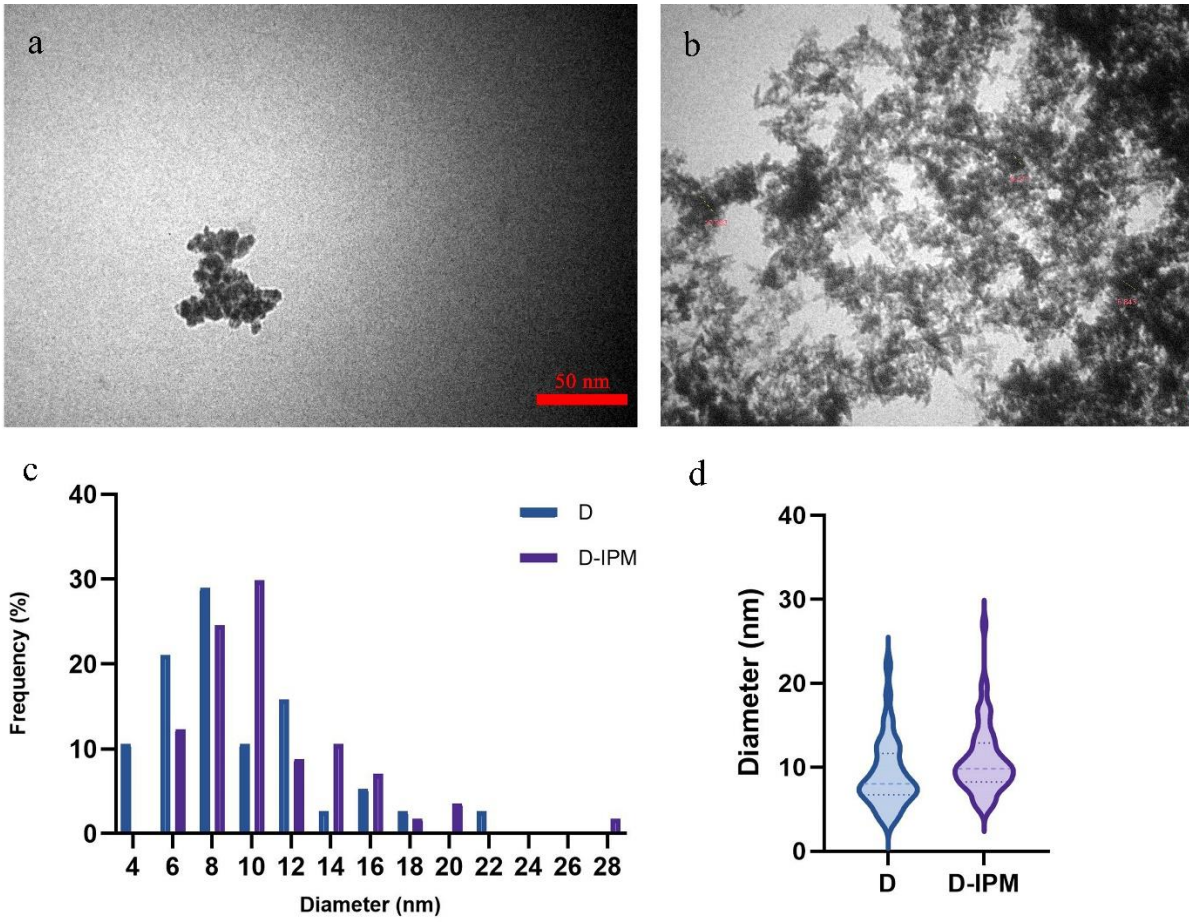


Fig. 2. TEM images of (a) dendrimers and (b) dendrimer–iopamidol conjugates, illustrating morphological changes following iopamidol loading. Particle size distribution of dendrimers (D) and dendrimer–iopamidol (D–IPM) is shown as (c) a histogram and (d) a violin plot, demonstrating a noticeable increase in average particle size after drug conjugation.

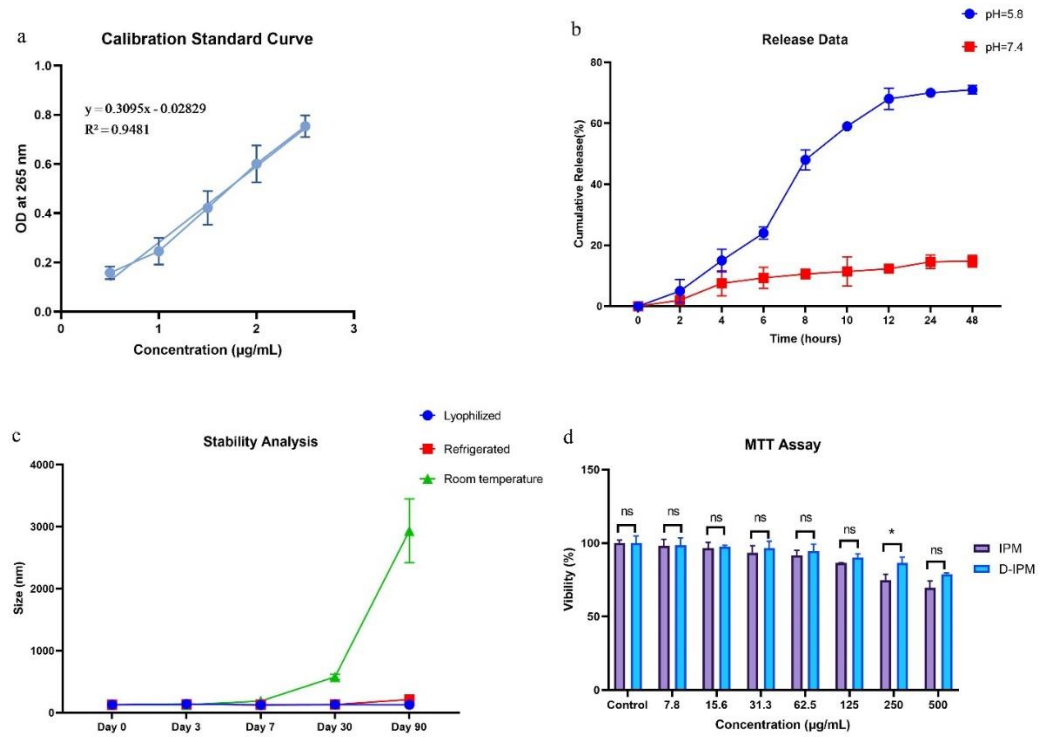


Fig. 3. (a) Calibration standard curve for iopamidol (IPM) demonstrating the relationship between concentration and absorbance. (b) Drug release profile of dendrimer-encapsulated iopamidol at two different pH values, 5.8 and 7.4, illustrating the pH-dependent release kinetics. (c) Stability analysis of the dendrimer-drug conjugate, monitored through changes in the hydrodynamic particle size over time and under various temperature conditions. (d) Cytotoxicity assessment of iopamidol (IPM) and dendrimer-encapsulated iopamidol (D-IPM) using the MTT assay at varying concentrations, showing the dose-dependent effects on cell viability. Data represent mean ± SD of three independent experiments (*p < 0.05; ns, non-significance).

Iopamidol Encapsulation Efficiency onto Dendrimers

The encapsulation efficiency of iopamidol onto the dendrimers was quantified using UV-Vis spectrophotometry. After establishing a standard calibration curve for iopamidol (Fig. 3a), the concentration of free iopamidol present in the supernatant was quantified. This allowed the indirect evaluation of the amount of iopamidol encapsulatet onto the dendrimers. On this basis, iopamidol encapsulation efficiency onto dendrimers was calculated as 43%. This value is considered acceptable, given that iopamidol was loaded onto the nanoparticles through non-covalent, non-ionic interactions. It compares favorably with previously reported encapsulating efficiencies of 30.6% and 33.3% for iodinated contrast agents loaded onto nanoparticles, although it is lower than the 85% achieved using crosslinking strategies. It is also higher than the approximately 30% encapsulating reported for PEG-core dendritic iobitridol conjugates (39-41, 44).

Iopamidol Release Profile from Dendrimer

Fig. 3b illustrates the pH-dependent release profile of iopamidol from the dendrimer–iopamidol complex. Release of iopamidol at pH 5.8 sustained and strongly time-dependent. There was no variation in the release of iopamidol from 0 to 2 h (mean difference = -5; p = 0.63). However, a significant increase in drug release was first observed at 4 h (mean difference = -15; ****p < 0.0001), with the increment becoming larger with each subsequent time interval up to 48 h. Maximum release was recorded at 48 h, with a mean difference of -71 compared to baseline (0 h), indicating a significant accumulation of released drug over time (****p < 0.0001 for all time points after 4 h).

At pH 7.4, the release profile of iopamidol was much slower and less steep than that at pH 5.8. While no significant increase in release was observed during the first 4 h, A significant increase in iopamidol release was observed at 6 h (mean difference = -9.3; **p = 0.0093). Cumulative iopamidol release increased steadily until 48 h, but the total release was still much less than that at pH 5.8 (mean difference = -14.8 at 48 h; ****p < 0.0001).

Tukey's test-supported multiple comparison analysis also evidenced a significant effect of pH and time on the release rate of iopamidol. The release difference between pH 5.8 and 7.4 was statistically significant from 6 h (****p < 0.0001). These findings confirm the pH-dependent release behavior of the dendrimer–drug complex and demonstrate enhanced drug release under acidic conditions.

Overall, the release of iopamidol from D-IPM was also pH-dependent, with more rapid release under mildly acidic conditions (pH 5.8), which mimics the tumor microenvironment. This pH-responsive release profile may facilitate passive accumulation and preferential drug release in acidic tumor microenvironments, This characteristic may provide an additional advantage over non-responsive formulations and complements active tumor-targeting strategies such as PMAI-PEG-RGD systems (37).

In Vitro Stability of the Dendrimer-Iopamidol Complex

Fig. 3c depicts the stability profile of the dendrimer-iopamidol complex under various storage conditions. A Tukey's multiple comparison test was used to compare changes in particle size across time points and conditions. No significant changes in hydrodynamic size were observed in samples stored under lyophilized or refrigerated conditions for 90 days. Consistent with this finding, all pairwise comparisons between these conditions were non-significant (p > 0.9999). Therefore, one of the advantageous features of the D-IPM system seemed to be good colloidal stability. Unlike gold nanoparticle–dendrimer hybrids that would suffer from redox-induced aggregation in CT imaging (45), our system was stable for over 90 days under refrigerated and lyophilized storage. Such stability is likely to be attributed to the absence of any redox-sensitive components and steric stabilization by PEG chains (46, 47).

In contrast, those stored at room temperature exhibited loss of stability in a time-dependent fashion. After 30 and 90 days of storage at room temperature, a statistically

Corrected Proof

significant increase in hydrodynamic size was observed compared with other storage conditions. The main time-dependent variations in storage conditions were as follows: (i) at day 30: lyophilized vs. room temperature (mean difference = -447.6 nm, 95% CI: -851.7 to -44.49, *p = 0.0193) and refrigerated vs. room temperature (mean difference = -447.1 nm, 95% CI: -851.2 to -42.99, *p = 0.0195); (ii) at day 90: lyophilized vs. room temperature (mean difference = -2804 nm, 95% CI: -3208 to -2400, ***p < 0.0001) and refrigerated vs. room temperature (mean difference = -2720 nm, 95% CI: -3124 to -2316, ***p < 0.0001). Generally, both cold storage and lyophilization effectively preserved the nanoscale features of the dendrimer-drug complex, while storage at room temperature for more than 30 days caused a loss of stability of D-IPM. Notably, previous studies also showed that PEG-core dendrimers are highly thermally stable after autoclaving (39). Accordingly, this platform may be stable across a wide range of temperatures.

In Vitro Biocompatibility

Tukey's post hoc test showed no significant difference in cell viability between untreated control cells and cells treated with lower concentrations of IPM (7.8-62.5 µg/mL). However, there was a significant decrease in viability at a concentration of 125 µg/mL (mean difference = 13.6, **p = 0.0091), 250 µg/mL (mean difference = 25.4, ****p < 0.0001), and 500 µg/mL (mean difference = 30.6, ****p < 0.0001). D-IPM also displayed the same cytotoxic pattern; although viability did not differ significantly between untreated controls and cells exposed to lower D-IPM concentrations (7.8-125 µg/mL), viability was significantly decreased at 250 µg/mL and 500 µg/mL (mean difference = 13.6, p = **0.0091 and mean difference = 21.1, ****p < 0.0001, respectively)**. These results indicated that dendrimer binding did not significantly alter the cytotoxic threshold of iopamidol.

Furthermore, pairwise comparisons of equivalent concentrations of IPM and D-IPM also showed no significant difference at 7.8, 15.6, 31.3, 62.5, 125, and 500 µg/mL between these two formulations (p > 0.05), indicating equivalent cytotoxic activity of free and dendrimer-bound drug formulations. However, a small, significant difference in the toxicity of the two formulations was observed at a concentration of 250 µg/mL, with higher viability reported for the dendrimer-bound group than for the free group (mean difference = 11.8, p = *0.0394).

Overall, these findings suggest that dendrimer encapsulation may reduce the cytotoxicity of iopamidol in HEK-293 cells, potentially due to the presence of PEG, which may modulate cellular uptake. These observations are consistent with previous reports on PMAI-PEG-RGD nanoparticles, which maintained more than 80% cell viability at concentrations up to 1000 µg/mL in both cancer (4T1) and normal (HUVEC) cell lines (37). Moreover, the slightly higher cell viability observed at higher concentrations suggests an improved safety profile compared with free iopamidol. This observation is consistent with previous studies showing that the conjugation or loading of iodine-based contrast agents onto nanoparticles can reduce their cytotoxicity (42-44).

In Vitro Contrast Enhancement with the Dendrimer-Iopamidol Complex

The mean CT attenuation values values are listed in Table 2. Free iopamidol produced a mean attenuation of 2483.61 ± 215.4 HU, but the dendrimer–iopamidol complex achieved a significantly higher value of 3985.06 ± 312.9 HU. Both values were significantly higher than that of the distilled water control (-70.87 ± 18.6 HU; p < 0.05). These data indicate that the dendrimer formulation greatly enhanced contrast efficiency compared to free iopamidol (Fig. 4).

Although iodine has a lower atomic number (Z = 53) than gold (Z = 79), the D-IPM system achieved an attenuation of 3985 HU at 150 mg I/mL. This value exceeded the ~3560 HU reported for PEGylated gold nanoparticles at 117 mg Au/mL (45). These findings suggest that the dendrimer formulation improves the imaging performance of iodine-based contrast agents, enabling high CT attenuation without relying on high-atomic-number materials.

Table 2. *In vitro* contrast enhancement of iopamidol and dendrimer-iopamidol.

Sample	Mean contrast (HU)
Dendrimer-Iopamidol	3985.057 ± 312.9
Iopamidol	2483.608 ± 215.4
Water (Control)	-70.872 ± 18.6

Corrected Proof

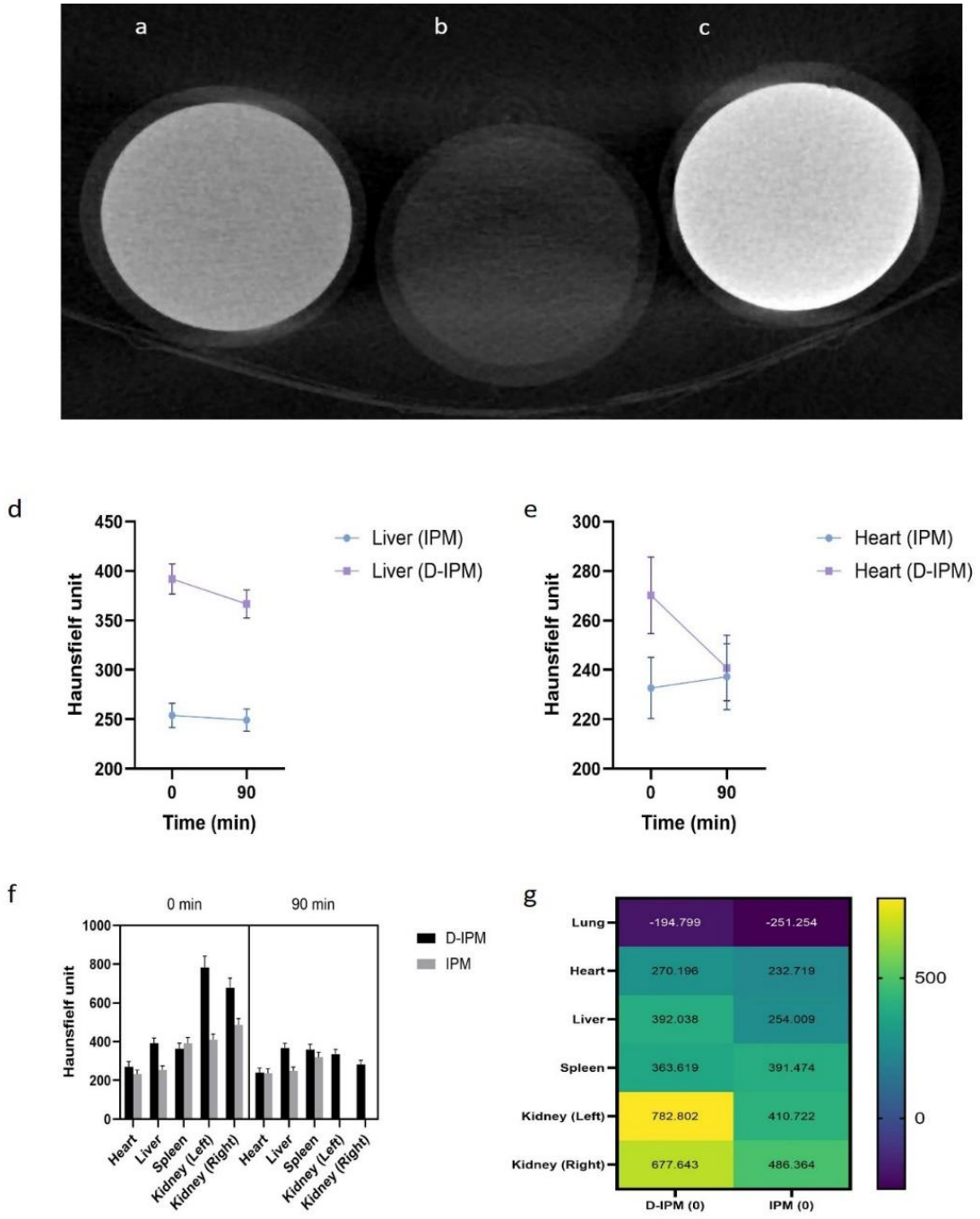


Fig. 4. *In vitro* contrast enhancement of (a) iopamidol, (b) distilled water, and (c) dendrimer-iopamidol. *In vivo* contrast enhancement in (d) liver and (e) heart tissues induced by iopamidol (IPM) and dendrimer-iopamidol (D-IPM). (f-g) Contrast enhancement in Hounsfield units (HU) for dendrimer-iopamidol (D-IPM) and iopamidol (IPM) at 0 and 90 min across various tissues.

In Vivo Findings

Renal and Bladder Clearance Profile

The distribution of free IPM and D-IPM in the kidneys and bladder was quantified at 0 and 90 min post-injection (Table 3). Free IPM had a rapid urinary tract excretion, which was evidenced by the highly elevated HU values in the bladder at the 0 min post-injection time point (HU = 3701 ± 215.8). This rapid excretion was accompanied by a moderate renal enhancement (HU = 410.7 ± 29.1 in the left kidney and 486.4 ± 32.7 in the right kidney). In contrast, D-IPM had slower clearance, as indicated by a reduced bladder accumulation (HU = 3173.3 ± 282.6 at baseline ($p > 0.0678$) and 1846.4 ± 175.4 at 90 min ($p < 0.0001$), as well as increased renal retention of the D-IPM group at baseline (HU = 782.8 ± 58.4; $p < 0.0001$ in the left kidney and HU = 677.643 ± 50.2; $p = 0.0017$ in the right kidney).

Table 3. Average contrast enhancement in Hounsfield units (HU) by iopamidol (IPM) and dendrimer-iopamidol (D-IPM) in different tissues at 0 and 90 min post-injection *in vivo*.

Organ	D-IPM (0 min)	D-IPM (90 min)	IPM (0 min)	IPM (90 min)
Lung	-194.799 ± 16.5	-361.445 ± 22.1	-251.254 ± 18.7	-300.227 ± 20.4
Heart	270.196 ± 26.8	240.779 ± 22.9	232.719 ± 21.4	237.324 ± 23.1
Liver	392.038 ± 26.5	366.873 ± 24.7	254.009 ± 21.3	249.193 ± 19.8
Spleen	363.619 ± 28.7	358.867 ± 27.4	391.474 ± 30.2	319.198 ± 25.1
Kidney (Left)	782.802 ± 58.4	335.254 ± 25.3	410.722 ± 29.1	-
Kidney (Right)	677.643 ± 50.2	282.238 ± 21.8	486.364 ± 32.7	-
Bladder	3173.318 ± 282.6	1846.355 ± 175.4	3701 ± 215.8	-

Target-to-Non-Target (T/NT) Ratio Analysis

To calculate organ-specific uptake, T/NT ratios were derived by dividing the HU values of the kidney and liver by those of the heart at 0 min. At 0 min, the left and right kidneys showed T/NT ratios of 2.90 and 2.51, respectively. The liver showed a T/NT ratio of 1.45 at 0 min and 1.52 at 90 min. These elevated T/NT ratios suggest preferential accumulation of D-IPM in the kidney and liver compared to the heart, indicating relatively greater accumulation in these organs than in the heart.

PEG-based nanoplatforms are of significant value in achieving the highest efficacy of Iodinated contrast media (ICMs) for CT imaging. PEGylation significantly improves nanoparticles' biocompatibility and blood half-life, thus facilitating longer imaging times and reducing renal toxicity (48, 49). The study further points out that PEG-based nanoplatforms are associated with improved biodistribution owing to their "stealth" properties that avoid recognition by the mononuclear phagocyte system. This prolongs systemic circulation and facilitates passive drug accumulation in target tissues, such as tumors, via the EPR effect. These features combined make PEG-based nanoparticles more suitable to target ICMs with enhanced contrast intensity and less systemic toxicity (50). For example, PEG12000–Gen4–IOB enabled long vascular enhancement by 32 min following injection of 450 mg I/kg in rats, while low-molecular-weight agents cleared after 5 min. Prolonged circulation was rationalized on the grounds of synergy between PEGylation and its higher molecular weight, minimizing extravasation, and renal filtration properties ideally suited for blood-pool imaging (39).

In Vivo CT Imaging

According to the three-dimensional (Fig. 5) and cross-sectional (Fig. 6) CT images of mice, the kidneys were clearly observable after the injection of dendrimer–iopamidol, as shown by blue arrows. On the other hand, after the administration of free iopamidol, most of the contrast agent was excreted quickly into the bladder (white arrows), resulting in poor visualization of the kidneys. This finding reflects increased persistence in the body and slower renal clearance of D-IPM compared to IPM. In addition, brighter spots in the images taken for D-IPM were identified corresponding to contrast agent concentration in various tissues, particularly the liver (orange arrows). These results correlated with the higher HU values of cardiac and hepatic tissues and greater than 1 target-to-non-target ratios for kidneys and liver, which indicates these as the major targets of D-IPM. At 90 min, there was still extensive hepatic uptake of D-IPM despite overall clearance from other organs. These images demonstrated the extended durability, greater retention, and better contrast potential of D-IPM compared to free IPM.

Although this study demonstrated the potential of the dendrimer–iopamidol system in enhancing CT imaging, its potential does not end with this modality. Thanks to the structural flexibility and tuneability of this PEG-based dendrimer, the nanosystem also has excellent potential to be used in other molecular imaging modalities such as magnetic resonance imaging (MRI) (29, 30, 51, 52). Previous studies showed that dendrimer conjugation with other contrast-enhancing agents, such as Gd^{3+}, can enable cellular uptake, improve image resolution, and reduce systemic toxicity for application in MRI (29, 30, 51, 52). Hence, the optimization of this nanosystem for use in various imaging platforms offers new ways of constructing multifunctional and platform-independent contrast agents for biomedical imaging.

Corrected Proof

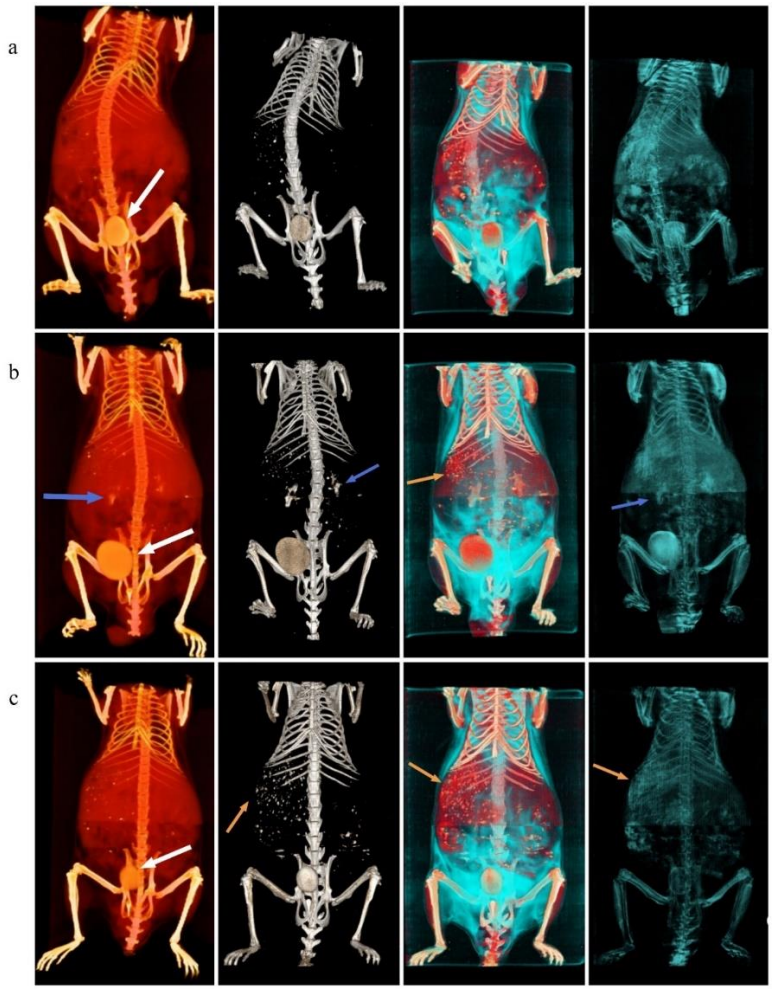


Fig. 5. Three-dimensional CT images of mice obtained immediately after injection of (a) free iopamidol and (b) dendrimer–iopamidol, as well as (c) 90 min post-injection of D-IPM.

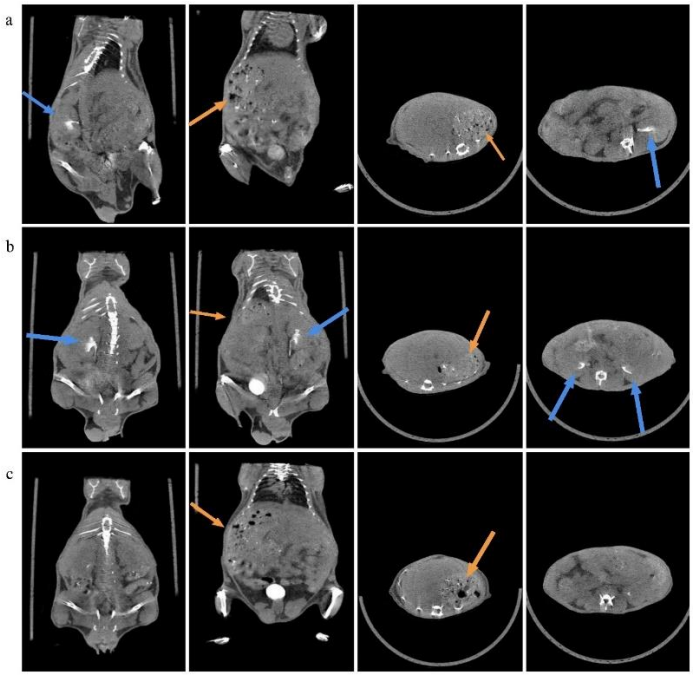


Fig. 6. Cross-sectional CT images of mice obtained immediately after injection of (a) free iopamidol and (b) dendrimer–iopamidol, as well as (c) 90 min post-injection of D-IPM.

CONCLUSION

In summary, our findings demonstrate efficient design and synthesis of a G2 dendrimer–iopamidol complex with better physicochemical stability, biocompatibility, and enhanced CT imaging performance. Its high iodine loading capacity, pH-responsive release, long-term *in vivo* stability, and superior contrast enhancement make D-IPM a potential candidate for developing next-generation CT contrast agents. Further investigations using tumor model- and disease-based models are necessary to investigate its diagnostic and translational potential.

ACKNOWLEDGEMENTS

Tehran University of Medical Sciences supported this study

CONFLICTS OF INTEREST

The authors declare no competing interests.

FUNDING

None.

DATA AVAILABILITY

None.

AUTHOR CONTRIBUTIONS

The manuscript was collaboratively authored by all contributors, who have all reviewed and endorsed the final version.

AI STATEMENT

During the preparation of this review, the authors utilized ChatGPT solely for grammar checking and refining readability. The content was not generated by AI; it was only used as a tool for enhancement. After applying these tools, the authors carefully reviewed and edited the content as necessary and take full responsibility for the material presented in this publication.

ETHICAL APPROVAL

All animal experiments adhered to the institutional ethical guidelines and were approved by Tehran University of Medical Sciences' Ethics Committees (Approval Code: IR.TUMS.AEC.1403.204) and Iran University of Medical Sciences' Ethics Committees (Approval Code: IR.IUMS.REC.1403.561).

REFERENCES

1. Sun Z, Silberstein J, Vaccarezza M. Cardiovascular computed tomography in the diagnosis of cardiovascular disease: beyond lumen assessment. J Cardiovasc Dev Dis. 2024;11(1):22.
2. So A, Nicolaou S. Spectral computed tomography: fundamental principles and recent developments. Korean J Radiol. 2021;22(1):86-96.
3. Parillo M, van der Molen AJ, Asbach P, Elsholtz FHJ, Laghi A, Ronot M, et al. The role of iodinated contrast media in computed tomography structured reporting and data systems (RADS): a narrative review. Quant Imaging Med Surg. 2023;13(11):7621-7631.
4. Spampinato MV, Abid A, Matheus MG. Current radiographic iodinated contrast agents. Magn Reson Imaging Clin N Am. 2017;25(4):697-704.
5. Joshi MP, Chaudhari A, Kharkar PS, Joshi SV. Chemistry of iodinated contrast media (ICM): A mini review. Mini Rev Org Chem. 2021;18(7):885-901.
6. Joaquim JJ, Matos C, Mateos-Campos R. Safety asssessment of iopromide contrast media: a narrative review focusing on adverse events. Curr Issues Pharm Med Sci. 2023;36(3):163-7.
7. England A, Rawashdeh M, Moore N, Young R, Curran G, McEntee MF. More sustainable use of iodinated contrast media - Why? Radiography (Lond). 2024;30 Suppl 1:74-80.
8. Lee T, Kim WK, Kim AJ, Ro H, Chang JH, Lee HH, et al. Low-osmolar vs. iso-osmolar contrast media on the risk of contrast-induced acute kidney injury: a propensity score matched study. Front Med (Lausanne). 2022;9:862023.
9. Andreucci M, Faga T, Pisani A, Sabbatini M, Russo D, Michael A. The choice of the iodinated radiographic contrast media to prevent contrast-induced nephropathy. Adv Nephrol. 2014;2014(1):691623.
10. Barrett BJ, Parfrey PS, Vavasour HM, O'Dea F, Kent G, Stone E. A comparison of nonionic, low-osmolality radiocontrast agents with ionic, high-osmolality agents during cardiac catheterization. N Engl J Med. 1992;326(7):431-436.
11. Mruk B. Renal safety of iodinated contrast media depending on their osmolarity–current outlooks. Pol J Radiol. 2016;81:157.
12. Solomon R. The role of osmolality in the incidence of contrast-induced nephropathy: a systematic review of angiographic contrast media in high risk patients. Kidney Int. 2005;68(5):2256-2263.
13. Katholi RE. Contrast-induced nephropathy-choice of contrast agents to reduce renal risk. Am Heart Hosp J. 2009;7(1):45-49.
14. Manual ACR. On contrast media. Virginia (VA), USA: American College of Radiology. 2020.
15. Bolten JS, Mancuso RV, Roos NJ, Mayr A, Puligilla RD, Kraus L, et al. Nephrotoxicity of iopamidol is associated with mitochondrial impairment in human cell and teleost models. Toxicol Appl Pharmacol. 2023;466:116493.
16. Asy'ari AH, Rahaju AS, Mustika A. Histopathology and renal function in wistar rats after intravascular injection of iodinated contrast media iohexol and iopamidol. Syntax Lit J Ilm Indones. 2022;7(1):361.
17. Shilo M, Reuveni T, Motiei M, Popovtzer R. Nanoparticles as computed tomography contrast agents: current status and future perspectives. Nanomedicine (Lond). 2012;7(2):257-269.

Corrected Proof

18. Cormode DP, Naha PC, Fayad ZA. Nanoparticle contrast agents for computed tomography: a focus on micelles. Contrast Media Mol Imaging. 2014;9(1):37-52.
19. De La Vega JC, Hafeli UO. Utilization of nanoparticles as X-ray contrast agents for diagnostic imaging applications. Contrast Media Mol Imaging. 2015;10(2):81-95.
20. Alamos-Musre S, Beltran-Chacana D, Moyano J, Marquez-Miranda V, Duarte Y, Miranda-Rojas S, et al. From structure to function: the promise of pamam dendrimers in biomedical applications. Pharmaceutics. 2025;17(7).
21. Fadaei MR, Fadaei MS, Kheirieh AE, Hatami H, Rahmanian-Devin P, Tayebi-Khorrami V, et al. Overview of dendrimers as promising drug delivery systems with insight into anticancer and anti-microbial applications. Int J Pharm X. 2025;10:100390.
22. Kanani-Jazi MH, Akbari S. Host–guest chemistry and functional versatility of dendritic nanomaterials in advanced applications. Nanoscale Adv Mater. 2025;2(2):111-120.
23. Derakhshan S, Shafiee Ardestani M, Zadeh Mehrizi T, Bitarafan-Rajabi A, Jokar S, Pirali Hamedani M, et al. (99m)Tc-SNW-1 nanoparticle labeling and its biodistribution/pathological evaluations. J Labelled Comp Radiopharm. 2025;68(9-10):e4160.
24. Rasoulianshiadehi M, Zadeh Mehrizi T, Eshrati B, Shafiee Ardestani M. Advances in targeted cancer imaging using galactose-modified polymeric nanoparticles: A systematic review. Iran J Nucl Med. 2026;34(1):32-47.
25. Ajdary N, Davoudi M, Zadeh Mehrizi T, Shafiee Ardestani M, Nequi Marnani H, Ebrahimi Shahmabadi H, et al. Development and characterization of colloidally stable dendrimer–botox conjugates for targeted muscle delivery and radiolabeled imaging. Pharm Sci. 2026;32(2):201-218.
26. Mohammadzadeh P, Cohan RA, Ghoreishi SM, Bitarafan-Rajabi A, Ardestani MS. AS1411 aptamer-anionic linear globular dendrimer g2-iohexol selective nano-theranostics. Sci Rep. 2017;7(1):11832.
27. Assadi A, Najafabadi VS, Shandiz SA, Boroujeni AS, Ashrafi S, Vaziri AZ, et al. Novel chlorambucil-conjugated anionic linear-globular PEG-based second-generation dendrimer: in vitro/in vivo improved anticancer activity. Onco Targets Ther. 2016;9:5531-5543.
28. Bober Z, Bartusik-Aebisher D, Aebisher D. Application of dendrimers in anticancer diagnostics and therapy. Molecules. 2022;27(10):3237.
29. Mirzaei M, Mehravi B, Ardestani MS, Ziaee SAM, Pourghasem P. In vitro evaluation of Gd 3+-anionic linear globular dendrimer-monoclonal antibody: potential magnetic resonance imaging contrast agents for prostate cancer cell imaging. Mol Imaging Biol. 2015;17:770-776.
30. Hashempour Alamdari N, Alaei-Beirami M, Sadat Shandiz SA, Hejazinia H, Rasouli R, Saffari M, et al. Gd3+-asparagine-anionic linear globular dendrimer second-generation G2 complexes: novel nanobiohybrid theranostics. Contrast Media Mol Imaging. 2017;2017(1):3625729.
31. Ajdary N, Shafiee Ardestani M, Nequi Marnani H, Eshrati B, Zadeh Mehrizi T. Current strategies in the development of nanoformulations to enhance the stability of botox: a systematic review. AAPS PharmSciTech. 2025;27(1):38.
32. Namazi H, Adeli M. Dendrimers of citric acid and poly (ethylene glycol) as the new drug-delivery agents. Biomaterials. 2005;26(10):1175-1183.
33. Ebrahimi S, Sadeghizadeh M, Aghasadeghi M, Shafiee Ardestani M, Behmanesh M. One-step synthesis of anionic peg-citrate G2 dendrimer and evaluation of its cytotoxicity in two cell lines. Pathobiol Res. 2015;17(4):13-24.
34. Haririan I, Alavidjeh MS, Khorramizadeh MR, Ardestani MS, Ghane ZZ, Namazi H. Anionic linear-globular dendrimer-cis-platinum (II) conjugates promote cytotoxicity in vitro against different cancer cell lines. Int J Nanomedicine. 2010;5:63-75.
35. Khosravy MS, Shafiee Ardestani M, Ahangari Cohan R, Doroud D, Amini S, Momen SB, et al. Design, synthesis, physicochemical and immunological characterization of dendrimer-HBsAg conjugate. Vaccine Res. 2014;1(2):24-28.
36. Pargoo EM, Aghasadeghi MR, Parivar K, Nikbin M, Rahimi P, Ardestani MS. Lamivudine-conjugated and efavirenz-loaded G2 dendrimers: Novel anti-retroviral nano drug delivery systems. IET Nanobiotechnol. 2021;15(7):627-637.
37. Gao C, Zhang Y, Zhang Y, Li S, Yang X, Chen Y, et al. cRGD-modified and disulfide bond-crosslinked polymer nanoparticles based on iopamidol as a tumor-targeted CT contrast agent. Polym Chem. 2020;11(4):889-899.
38. Shah S, Rangaraj N, Singh SB, Srivastava S. Exploring the unexplored avenues of surface charge in nano-medicine. Colloid Interface Sci Commun. 2021;42:100406.
39. Fu Y, Nitecki DE, Maltby D, Simon GH, Berejnoi K, Raatschen HJ, et al. Dendritic iodinated contrast agents with PEG-cores for CT imaging: synthesis and preliminary characterization. Bioconjug Chem. 2006;17(4):1043-1056.
40. Yin Q, Yap FY, Yin L, Ma L, Zhou Q, Dobrucki LW, et al. Poly(iohexol) nanoparticles as contrast agents for in vivo X-ray computed tomography imaging. J Am Chem Soc. 2013;135(37):13620-13623.
41. Kale T, Bendale K, Singh KK, Chaudhari P. Albumin based iohexol nanoparticles for computed tomography: an in vivo study. J Biomed Nanotechnol. 2019;15(2):236-247.
42. Balegamire J, Vandamme M, Chereul E, Si-Mohamed S, Azzouz Maache S, Almouazen E, et al. Iodinated polymer nanoparticles as contrast agent for spectral photon counting computed tomography. Biomater Sci. 2020;8(20):5715-5728.
43. Jeong Y, Jin M, Kim KS, Na K. Biocompatible carbonized iodine-doped dots for contrast-enhanced CT imaging. Biomater Res. 2022;26(1):27.
44. Alhasan A, Tajuddin HA, Sani SFA, Ali TH, Hisham S, Mokti MH, et al. Iohexol functionalized Si-Ag: Mn3O4

Corrected Proof

hybrid nanoparticles based contrast agent for computed tomography imaging. Mater Today Commun. 2022;33:104377.
45. Kojima C, Umeda Y, Ogawa M, Harada A, Magata Y, Kono K. X-ray computed tomography contrast agents prepared by seeded growth of goldnanoparticles in pegylated dendrimer. Nanotechnol. 2010;21(24):245104.
46. Feng SJ, Liu CH, Xia XM, Yu BY, Chu GW, Li H, et al. Unraveling the role of pegylation in the anti-aggregation stability of lipid nanoparticles. Nanoscale. 2025;17(47):27530-27537.
47. Bharadwaj P, Roullin VG, Chain JL. Crossing the blood-brain barrier: advances in dendrimer-based nanocarriers for central nervous system delivery. Nanoscale. 2025;17(40):23202-23227.
48. Chen Y, Su Y-C, Roffler SR. Polyethylene glycol immunogenicity in nanomedicine. Nat Rev Bioeng. 2025;3(9):742-760.
49. Devkota L, Bhavane R, Badea CT, Tanifum EA, Annapragada AV, Ghaghada KB. Nanoparticle contrast agents for photon-counting computed tomography: recent developments and future opportunities. Wiley Interdiscip Rev Nanomed Nanobiotechnol. 2025;17(1):e70004.
50. Zhang P, Ma X, Guo R, Ye Z, Fu H, Fu N, et al. Organic nanoplatforms for iodinated contrast media in ct imaging. Molecules. 2021;26(23):7063.
51. Mahdavimehr M, Rahdari T, Nikfarjam N, Ehtesham S, Shafiee Ardestani M, Asghari SM. Development and application of dual-modality tumor-targeting SPIONs for precision breast cancer imaging. Biomater Adv. 2025;172:214236.
52. Mohammadi E, Amanlou M, Sadat Ebrahimi SE, Hamedani MP, Mahrooz A, Mehravi B, et al. Cellular uptake, imaging and pathotoxicological studies of a novel Gd[iii]–DO3A-butrol nano-formulation. RSC Adv. 2014;4(86):45984-45994.

Corrected Proof